Positive and negative sequence current injection to improve voltages under unbalanced faults

Fill this

***Abstract*—Grid faults constitute a series of unfortunate events that compromise power systems. With the increasing integration of renewables and their associated power electronics converters, the injected currents are controllable, but at the same time, they have to be limited so as not to damage the semiconductors. This poses the challenge to determine the combination of currents that improves the voltages at the point of common coupling. In this paper, such an issue is approached from an optimization perspective. Solving the optimization problem allows comparing its solutions with respect to the ones obtained by following the grid code control laws. Two fundamental scenarios are presented: one with a single converter, and another with two converters. Several parameters are varied for all kinds of faults to spot the changes on the currents, such as the severity of the fault, the distance of a hypothetical submarine cable, and the resistive/inductive ratio of the impedances. Overall, the results indicate that injecting only reactive power is not always the preferable choice. However, grid codes can be regarded as near-optimal decision rules, since their solution only differs slightly from the optimal one.**

***Index Terms*—VSC, Grid-Support, Reference Optimization, Asymmetrical Fault, Current Saturation**

I. Introduction

THE rise in renewable energies has carried along with it the inclusion of Voltage Source Converters (VSC) as a means of coupling energetic resources to the grid while providing controllability [1]–[3]. Adopting such power electronics equipment has induced a progressive shrinkage on synchronous generators' influence in power systems. The high flexibility of VSC control enables advanced grid-support control, which could enhance the system performance during the fault and ensure a fast recovery after the fault clearance. However, compared to electrical machines, VSCs cannot withstand overloads [4]. Indeed, current (and also voltage) limitations cause VSC to behave differently. They reach what is called a saturated state. Many equilibrium points may arise as a result of that, especially in grids formed by multiple converters operating in critical conditions. The solution to such systems is also likely to become an arduous task to compute, as saturation states are defined by non-linear equations, or in more detail, by piecewise functions.

Not only do currents have to be constrained to not exceed the limitations, but they also have to collaborate on improving the voltages [5]. This becomes visible when looking at the requirements imposed by Transmission System Operators (TSO) in its grid codes [6], [7]. Although this was not the case years ago, when wind power represented a small percentage of the electricity mix, nowadays wind power plants have to control active and reactive power [8]. Besides, they have to transiently support the faults. The latter aspect is often referred to as low voltage ride through (LVRT) [9], [10]. The traditional approach to raise the voltage at the point of common coupling is to inject reactive power proportionally to the severity of the fault [8], [11]. During the analysis of faults, it is often the case that voltages are decomposed into positive, negative, and zero sequence values. By doing so, the study of the fault is expected to be simplified, and in addition to that, some intuition can be built from inspecting the positive and negative sequence voltages. A concerning unbalanced fault is such that substantially decreases the positive sequence voltage with respect to the nominal voltage while the negative sequence voltage increases. Both sequences have to be thoroughly controlled, as discussed in [11], [12].

Nevertheless, for the most part, grid codes only specify reactive power injection during faults [13], [14]. This is because transmission networks are often considered to have an inductive characteristic. The influence of the grid impedance characteristics of the system optimized under an equilibrium state is covered in [12], where the authors express the currents to inject as a function of the voltage and the impedances. A recursive relation between the voltage and the current is found, which invalidates the possibility of working with a closed-form expression from where to compute the optimal currents solution. Expressions of the same nature are proposed in [15], where instead of attempting to solve the optimization problem, a control parameter is introduced. This takes various values, but no analysis is carried out to determine the optimal choice. The effect of varying this control parameter is studied in [16], although it is not computed with a systematic approach, but rather, manually. Reference [17] proposes a maximum allowed support (MAS) control scheme that is said to provide the maximum voltage support and simultaneously satisfying the current limitations. The study does not explicitly indicate how the current is distributed among the real and the imaginary positive and negative sequence components, and variations in input parameters are rather limited. Another voltage support scheme is presented in [18], where the injected currents depend neither on the active power nor the filter resistance. In addition, positive and negative sequence grid voltage values are imposed, which facilitates the obtention of the steady-state current values. A variation of the grid code requirements is depicted in [19]. The authors found it to provide better results than conventional grid codes. The majority of the grid support strategies described above are compared and summarized in [20]. It is worth mentioning that the systems under study considered in these references include a single VSC. Further conclusions are expected to be extracted from examining a two-converter case study.

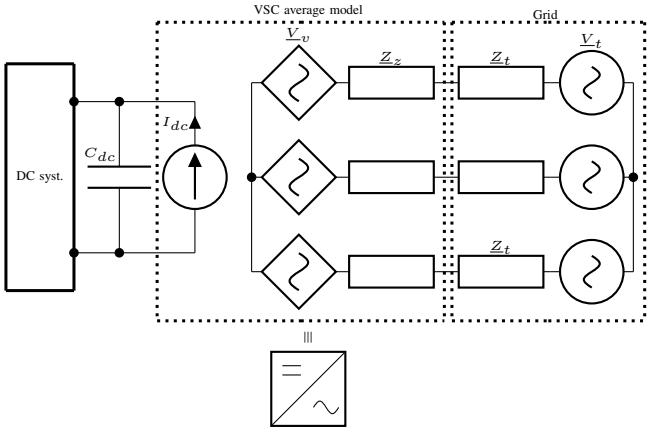

Fig. 1: Average model of a VSC connected to the grid

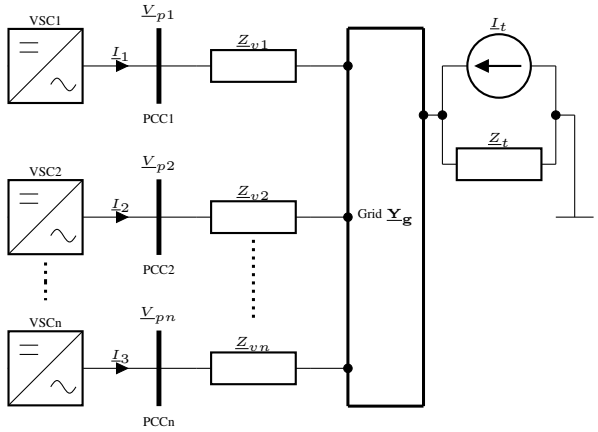

Fig. 2: Single-phase representation of a complete system

This paper proposes a methodology to identify the optimized system equilibrium point during the fault considering converters' current limitations. Two other control rules are implemented. They both follow the conventional droop profile found in grid codes, yet one prioritizes positive sequence current whereas the other prioritizes negative sequence current. The two of them are restricted to only injecting reactive power. These three options are tested for both balanced and unbalanced faults, where this last category includes the line to ground and the line to line fault. First, a basic system with a single converter is studied. Then, the analysis is repeated for a system with two converters in order to identify their interaction in saturated states.

This paper presents two main contributions. On the one hand, it indicates the preferable injected currents under diverse conditions. A deeper understanding of the optimality of the solutions is expected to be gained from it. On the other hand, comparisons between the optimal solution and the one obtained by following the grid code are presented. An assessment about the convenience of grid codes to support faults can be derived, which should be useful when proposing future modifications in order to evolve towards more resilient grids.

II. Formulation

A. System modeling

VSCs are elements that interconnect DC systems with AC systems. As shown in Fig. 1, they can be modeled following the so-called average model, where the switchings of the semiconductors are excluded. The VSC has been assumed to be connected to the AC grid with a filter in between denoted by $\underline{Z}_z$. The control strategy of the VSC consists of adjusting the voltages appropriately so that currents can indirectly meet the references [21].

Power systems are likely to involve more than a single converter. Therefore, the modeling is approached from a generalized perspective. Fig. 2 presents the modeling for a system with n converters. They are connected to a grid which has been split into a passive part, only formed by impedances and denoted by its admittance matrix $\underline{\mathbf{Y}}_{\mathbf{g}}$, and an active part, modeled with a Norton equivalent. Compared to dealing with a Thevenin equivalent, the Norton equivalent simplifies the formulation since it does not create an additional bus. The VSCs are treated as current sources that inject currents of the form of $\underline{I}_k \forall k \in [1, ..., n]$. Additional impedances denoted by $\underline{Z}_{vk}$ connect the point of common coupling to the grid. Such point of common coupling is precisely where the voltages ought to be improved.

The relationship between currents and voltages can be established with an analysis in the natural reference frame or by employing symmetrical components as in [22]. Although both approaches are equally valid, working in the natural reference frame allows studying the system with greater flexibility, as only the particular elements of the admittance matrices that depend on the fault admittance experience changes. No other modifications in the topology have to be considered. Consequently, voltages and currents are related by

$$\begin{pmatrix} \underline{\mathbf{I_1}} \\ \underline{\mathbf{I_2}} \\ \vdots \\ \underline{\mathbf{I_n}} \\ \underline{\mathbf{I_t}} \end{pmatrix} = \begin{pmatrix} \underline{\mathbf{Y_{v1}}} & \mathbf{0} & \dots & \mathbf{0} & -\underline{\mathbf{Y'_{v1}}} \\ \mathbf{0} & \underline{\mathbf{Y_{v2}}} & \dots & \mathbf{0} & -\underline{\mathbf{Y'_{v2}}} \\ \vdots & \vdots & \ddots & \vdots & \vdots \\ \mathbf{0} & \mathbf{0} & \dots & \underline{\mathbf{Y_{vn}}} & -\underline{\mathbf{Y'_{vn}}} \\ -\underline{\mathbf{Y'^{T}_{v1}}} & -\underline{\mathbf{Y'^{T}_{v2}}} & \dots & -\underline{\mathbf{Y'^{T}_{vn}}} & \underline{\mathbf{Y_g}} \end{pmatrix} \begin{pmatrix} \underline{\mathbf{V_{p1}}} \\ \underline{\mathbf{V_{p2}}} \\ \vdots \\ \underline{\mathbf{V_{pn}}} \\ \underline{\mathbf{V_g}} \end{pmatrix}. \tag{1}$$

For a given converter k, its injected currents and its associated voltages at the point of common coupling are further developed as

$$\begin{cases} \underline{\mathbf{I_k}} = \left[\underline{I}_k^{(a)}, \underline{I}_k^{(b)}, \underline{I}_k^{(c)}\right]^T \\ \underline{\mathbf{V_{pk}}} = [\underline{V}_{pk}^{(a)}, \underline{V}_{pk}^{(b)}, \underline{V}_{pk}^{(c)}]^T \end{cases} \tag{2}$$

i.e., they contain the a, b and c phase values. Since VSCs cannot inject zero sequence currents, the formulation of the problem also imposes

$$\underline{I}_k^a + \underline{I}_k^b + \underline{I}_k^c = 0 \ \forall k \in [1, ..., n] \ . \tag{3}$$

Voltages and currents are related via admittance matrices of the form $\underline{\mathbf{Y}}_{\mathbf{vk}}$, which in normal operating conditions follow

$$\underline{\mathbf{Y_{vk}}} = \begin{pmatrix} \frac{1}{\underline{Z}_{vk}} & 0 & 0 \\ 0 & \frac{1}{\underline{Z}_{vk}} & 0 \\ 0 & 0 & \frac{1}{\underline{Z}_{vk}} \end{pmatrix} \ . \tag{4}$$

In case a fault occurs at the buses interconnected by $\underline{Z}_{vk}$, elements $1/\underline{Z}_f$ are added by observation, where $\underline{Z}_f$ denotes the fault impedance.

On the contrary, the admittance matrix $\underline{\mathbf{Y}}_{\mathbf{g}}$ is a $3n_g \times 3n_g$ matrix also built by observation, where n_g is the number of buses found in this passive $\underline{\mathbf{Y}}_{\mathbf{g}}$ grid. The object $\mathbf{I_t}$ is a vector of dimensions $3 \times n_g$ which accounts for the injected currents into the grid denoted by $\underline{\mathbf{Y}}_{\mathbf{g}}$. All its elements are null except for three entries that consider the injected currents from the Norton equivalent of the grid. Matrices of the form $\underline{\mathbf{Y}}'_{\mathbf{vk}}$ are $3 \times 3n_g$ objects constituted by elements $1/\underline{Z}_{vk}$. In a realistic scenario, the grid $\underline{\mathbf{Y}}_{\mathbf{g}}$ may be partially constituted by active and reactive power loads, i.e., PQ buses. They can be either ignored if the current they consume is assessed to be comparatively smaller than the fault current, or they can be modeled as constant admittances. No PQ loads have been considered in the case studies shown in this paper.

The final goal of the modeling is the obtention of voltages. They are computed from (1) by operating the product between the inverse of the full admittance matrix and the currents' vector. In order to have a clearer comprehension of the voltages, they are eventually converted into symmetrical components by means of Fortescue's transformation [23]:

$$\begin{pmatrix} \underline{V}^0_{pk} \\ \underline{V}^+_{pk} \\ \underline{V}^-_{pk} \end{pmatrix} = \frac{1}{3} \begin{pmatrix} 1 & 1 & 1 \\ 1 & a & a^2 \\ 1 & a^2 & a \end{pmatrix} \begin{pmatrix} \underline{V}^a_{pk} \\ \underline{V}^b_{pk} \\ \underline{V}^c_{pk} \end{pmatrix} \ , \tag{5}$$

where $a = e^{j\frac{2\pi}{3}}$.

B. Optimization problem

Positive sequence voltages have to be maximized while negative sequence voltages have to be minimized. The zero sequence component of the voltages is a magnitude likely to become non-null under asymmetrical faults. Nevertheless, as VSCs are unable to inject zero sequence currents, it will remain an uncontrolled variable in the sense that no efforts will be made towards reducing it. Current saturation restrictions imposed by the VSC characteristics have to be respected. This applies to each phase of each converter. Therefore, the generic optimization problem is

$$\begin{aligned} \min_{\underline{I}} \quad & \sum_{k=1}^{n} \left[\lambda_k^+ |(1 - |\underline{V}^+_{pk}(\underline{I})|)| + \lambda_k^- |(0 - |\underline{V}^-_{pk}(\underline{I})|)| \right] \ , \\ \text{s.t.} \quad & \max(\underline{I}^a_k, \underline{I}^b_k, \underline{I}^c_k) \leq I_{\text{max,k}} \ \forall k \in [1, ..., n] \ , \end{aligned} \tag{6}$$

where λ_k^+ and λ_k^- are weighting factors, the positive and negative sequence components of voltages $\underline{V}_{pk}$ are symbolically expressed as functions of the currents, and $I_{\text{max,k}}$ is the maximum allowed current by the k converter. It has been assumed that voltages at each phase of the converter do not surpass the limitations, which seems a fair assumption considering that voltages decrease substantially during faults. Ignoring voltage limitations tends to be a commonality in the literature as well.

The results gathered in this paper are computed with Python 3.9.1 and the aid of the Mystic package, a highly constrained non-convex optimization framework [24], [25]. A differential global optimization solver has been employed with a relative precision up to $1e-6$.

C. Grid code rules

In order to improve voltages during faults, grid code control rules typically impose injections of currents proportional to the voltage drop [8], [26]. When defined as generic piecewise functions, for the positive sequence

$$\begin{cases} |\underline{I}^+_k| = 0 & |\underline{V}^+_{pk}| \geq V^+_{\text{high}} \\ |\underline{I}^+_k| = k_p(V^+_{\text{high}} - |\underline{V}^+_{pk}|) & V^+_{\text{low}} \leq |\underline{V}^+_{pk}| < V^+_{\text{high}} \\ |\underline{I}^+_k| = I_{\text{max},k} & |\underline{V}^+_{pk}| < V^+_{\text{low}} \end{cases} \tag{7}$$

whereas for the negative sequence

$$\begin{cases} |\underline{I}^-_k| = 0 & |\underline{V}^-_{pk}| \leq V^-_{\text{low}} \\ |\underline{I}^-_k| = k_n(|\underline{V}^-_{pk}| - V^-_{\text{low}}) & V^-_{\text{low}} < |\underline{V}^-_{pk}| \leq V^-_{\text{high}} \\ |\underline{I}^-_k| = I_{\text{max},k} & |\underline{V}^-_{pk}| > V^-_{\text{high}} \end{cases} \tag{8}$$

where the values of the constants are gathered in Table IV. Constants k_p and k_n, which represent the slope of the droop, are set as fixed quantities. The converter would therefore operate at saturated conditions during extreme faults because either the positive sequence voltage would reach the lower threshold V^+_{low} or the negative sequence voltage would surpass the upper threshold V^-_{high}. However, in severe faults, it is still possible that both limits are surpassed, or at least, approached. In case (7) and (8) were applied simultaneously, the required current to be injected by the VSC could potentially exceed the $I_{\text{max},k}$ limitation. Thus, it makes sense to establish a prioritization.

This paper considers the two straightforward prioritizations. One strategy is to have the positive sequence current following (7) and injecting the maximum allowed negative sequence current so as not to exceed the current limitations in any phase. This methodology will be commonly referred to as GCP. The other option, abbreviated as GCN, is concerned with obeying (8) and analogously injecting the maximum positive sequence current that respects the limits. During all situations, the converters work under saturated conditions (current limits reached) as the non-prioritized current is set to the allowed maximum. Also, only reactive power is injected. The procedure to determine the non-prioritized current is depicted below.

Consider a generic distribution of positive and negative sequence voltages in the complex plane, as in Fig. 3. Phase currents are related to zero, positive, and negative sequence components by

$$\begin{pmatrix} \underline{I}_a \\ \underline{I}_b \\ \underline{I}_c \end{pmatrix} = \begin{pmatrix} 1 & 1 & 1 \\ 1 & \underline{a}^2 & \underline{a} \\ 1 & \underline{a} & \underline{a}^2 \end{pmatrix} \begin{pmatrix} \underline{I}^0 \\ \underline{I}^+ \\ \underline{I}^- \end{pmatrix} \tag{9}$$

where $\underline{I}^0$ is null as the VSC is incapable of injecting it. The k index related to identifying a given VSC has been omitted to alleviate the notation. Explicitly, (9) becomes

$$\begin{cases} \underline{I}_a = \underline{I}^+ + \underline{I}^- \\ \underline{I}_b = \underline{a}^2\underline{I}^+ + \underline{a}\underline{I}^- \\ \underline{I}_c = \underline{a}\underline{I}^+ + \underline{a}^2\underline{I}^- \end{cases} \tag{10}$$

Then, the absolute value of the three-phase currents is set to the limit I_{max}. The goal of doing so is to determine the maximum current that causes one phase to reach saturation while the two others operate under the limits. This will act as the most restrictive option. Consequently, squaring the currents yields

$$\begin{cases} I_{\text{max}}^2 = (I_{re}^+ + I_{re}^-)^2 + (I_{im}^+ + I_{im}^-)^2 \\ I_{\text{max}}^2 = (-\frac{1}{2}I_{re}^+ + \frac{\sqrt{3}}{2}I_{im}^+ - \frac{1}{2}I_{re}^- - \frac{\sqrt{3}}{2}I_{im}^-)^2 \\ \qquad +(-\frac{1}{2}I_{im}^+ - \frac{\sqrt{3}}{2}I_{re}^+ - \frac{1}{2}I_{im}^- + \frac{\sqrt{3}}{2}I_{re}^-)^2 \\ I_{\text{max}}^2 = (-\frac{1}{2}I_{re}^+ - \frac{\sqrt{3}}{2}I_{im}^+ - \frac{1}{2}I_{re}^- + \frac{\sqrt{3}}{2}I_{im}^-)^2 \\ \qquad +(\frac{\sqrt{3}}{2}I_{re}^+ - \frac{1}{2}I_{im}^+ - \frac{\sqrt{3}}{2}I_{re}^- - \frac{1}{2}I_{im}^-)^2 \end{cases} \tag{11}$$

It can be seen that each phase current, set at the allowed maximum, depends on four components, that is, I_{re}^+, I_{im}^+, I_{re}^- and I_{im}^-. When the positive sequence is prioritized (GCP), the grid code rules in (7) determine the absolute value of the positive sequence current while its direction in the complex plane is extracted by shifting it $-\frac{\pi}{2}$ with respect to $\underline{V}^+$, as seen in Fig. 3. Thus, I_{re}^+ and I_{im}^+ would be known beforehand, and only the two remaining components I_{re}^- and I_{im}^- have to be computed from (11) for each phase. To do so, one component has to be expressed as a function of the other. This carries no extra complexity considering that phasor $\underline{V}^-$ is fully known, and so the direction of $\underline{I}^-$ has to be shifted $\frac{\pi}{2}$ from it. Making use of the relation

$$\tan(\alpha^-) = \frac{I_{im}^-}{I_{re}^-} \ , \tag{12}$$

current I_{im}^- can be expressed as a function of I_{re}^-, for instance, and therefore there is only one unknown in each expression of (11). Then, the resulting quadratic equations are solved for I_{re}^- and the associated I_{im}^- is found with (12).

Note that six $[I_{re}^-, I_{im}^-]$ pairs of solutions would be obtained in total. Three of them have to be discarded because they do not follow the pre-established direction of $\underline{I}^-$ (due to the quadratic characteristic of (11)). Out of the remaining three, the one with the smallest absolute value is picked. This way it is ensured that current saturation is only reached in one phase, while the other two operate below their limits.

An analogous procedure as the one described above applies to computing the positive sequence current in case the negative sequence component is prioritized (GCN).

D. Summary of support techniques

The paper evaluates and compares three support strategies, which are:

- OPT: corresponds to the solution of the optimization problem in (6), particularized for each system. It provides, by definition, the best solution. Both active and reactive powers can be injected.
- GCP: is the application of the grid code rule shown in (7). It prioritizes positive sequence current injection.
- GCN: follows the grid code negative sequence current injection shown in (8). Just like GCP, the current limitation is reached in one phase, and only reactive power can be injected.

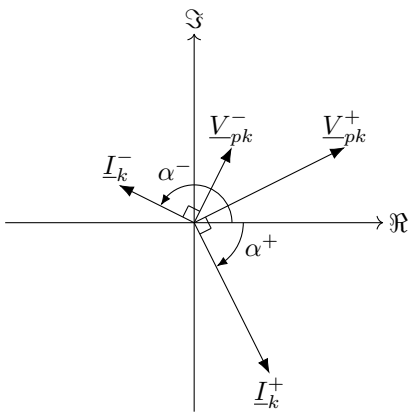

Fig. 3: Overview of positive and negative sequence voltages and currents following grid code rules

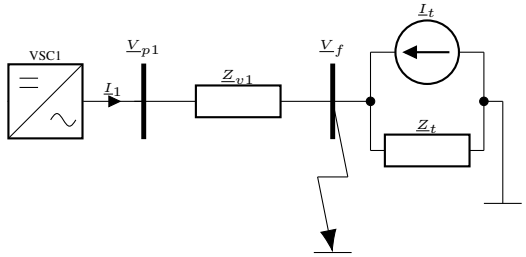

Fig. 4: Single-phase representation of the single converter system under study

III. Single converter case study

The analysis is first performed considering a one-converter case study as the one depicted in Fig. 4. A fault is caused at the point of connection of the grid. The impedances that model the fault are set accordingly to the type of fault, i.e., balanced or unbalanced (line to ground or line to line). Double line to ground faults are not covered in this study, not because they are unfeasible to be studied, but because there is a direct connection between the two faulted phases. This causes variations from a parametric study to have an almost null influence on the results. In any case, the goal is to improve the voltage $\underline{V}_{p1}$ by injecting the optimal $\underline{I}_1^a$, $\underline{I}_1^b$ and $\underline{I}_1^c$ currents.

Three parametric studies are performed. One considers variations in the fault impedance. This case is explicitly described in order to exemplify the formulation. Another study analyzes a varying R_1/X_1 ratio, which stands for the proportion between the resistive and the inductive parts that compose the impedance $\underline{Z}_{v1}$. This ratio is modified while the absolute value of the impedance is kept constant. The third case presents the effect of increasing the distance of a hypothetical submarine cable.

A. Fault impedance variation analysis

For a single converter system as the one depicted in Fig. 4, the fault impedance connected to the bus at voltage $\underline{V}_f$ is

TABLE I: System parameters for the one-converter case

Parameter	Value
$\underline{V}_t$	1.00
$I_{\max}$	1.00
$\underline{Z}_{v1}$	$0.01 + j0.05$
$\underline{Z}_t$	$0.01 + j0.1$
$[\lambda_1^+, \lambda_1^-]$	$[1, 1]$

responsible for identifying the fault. Explicitly, voltages and currents are related by

$$\begin{pmatrix} \underline{I}_1^a \\ \underline{I}_1^b \\ \underline{I}_1^c \\ \underline{I}_t^a \\ \underline{I}_t^b \\ \underline{I}_t^c \end{pmatrix} = (\underline{\mathbf{Y}}_\mathbf{v} + \underline{\mathbf{Y}}_\mathbf{f}) \begin{pmatrix} \underline{V}_{p1}^a \\ \underline{V}_{p1}^b \\ \underline{V}_{p1}^c \\ \underline{V}_f^a \\ \underline{V}_f^b \\ \underline{V}_f^c \end{pmatrix}, \tag{13}$$

where the admittance matrix has been split into two parts: $\underline{\mathbf{Y}}_\mathbf{v}$ represents the non-faulted admittance matrix of the system, whereas $\underline{\mathbf{Y}}_\mathbf{f}$ is constituted by the admittances that intervene in the fault. This way, the admittance matrices are defined as

$$\underline{\mathbf{Y}}_\mathbf{v} = \begin{pmatrix} \underline{Y}_{v1} & 0 & 0 & -\underline{Y}_{v1} & 0 & 0 \\ 0 & \underline{Y}_{v1} & 0 & 0 & -\underline{Y}_{v1} & 0 \\ 0 & 0 & \underline{Y}_{v1} & 0 & 0 & -\underline{Y}_{v1} \\ -\underline{Y}_{v1} & 0 & 0 & \underline{Y}_{v1} + \underline{Y}_t & 0 & 0 \\ 0 & -\underline{Y}_{v1} & 0 & 0 & \underline{Y}_{v1} + \underline{Y}_t & 0 \\ 0 & 0 & -\underline{Y}_{v1} & 0 & 0 & \underline{Y}_{v1} + \underline{Y}_t \end{pmatrix} \tag{14}$$

where $\underline{Y}_{v1} = 1/\underline{Z}_{v1}$ and $\underline{Y}_t = 1/\underline{Z}_t$.

On the other hand, the fault admittance $\underline{\mathbf{Y}}_\mathbf{f}$ is fully dependent on the fault, and therefore, it is built by observation. The optimization problem for the one case converter reads

$$\begin{aligned} \min_{\underline{I}_1^a, \underline{I}_1^b, \underline{I}_1^c} \quad & \lambda_1^+ |(1 - |\underline{V}_{p1}^+(\underline{I}_1^a, \underline{I}_1^b, \underline{I}_1^c)|)| \\ & + \lambda_1^- |(0 - |\underline{V}_{p1}^-(\underline{I}_1^a, \underline{I}_1^b, \underline{I}_1^c)|)| \ , \\ \text{s.t.} \quad & \max(\underline{I}_1^a, \underline{I}_1^b, \underline{I}_1^c) \leq I_{\max,1} \ , \end{aligned} \tag{15}$$

Because of the nature of the converter, it is also imposed that the sum of the three-phase currents becomes null. The procedure to solve the optimization problem is first responsible for initializing the admittances matrices $\underline{\mathbf{Y}}_\mathbf{v}$ as in (14), and then, constructing $\underline{\mathbf{Y}}_\mathbf{f}$. Next, currents are initialized to a random array of values, for instance. The Mystic package is subsequently called to solve the optimization problem stated in (15) up to a given relative precision δ, being $\delta = 1e-6$ for example. Positive and negative sequence voltages are evaluated to determine the optimality of the solution by means of (5). In the case of sweeping a range of n scenarios, this process is repeated n times. Currents are eventually also transformed to positive and negative sequence values since the final goal is to evaluate their values in this frame of reference. Unless noted otherwise, the corresponding baseline parameters of the system in Fig. 4 are indicated in Table I.

Solving the problem with the aforementioned steps for a balanced fault yields the results shown in Fig. 5, where impedance $\underline{Z}_x$ denotes the fault impedance connected to each phase. The results suggest that the OPT case is the preferred one, as its associated objective function is always the smallest, as expected. This optimal solution is achieved by distributing the

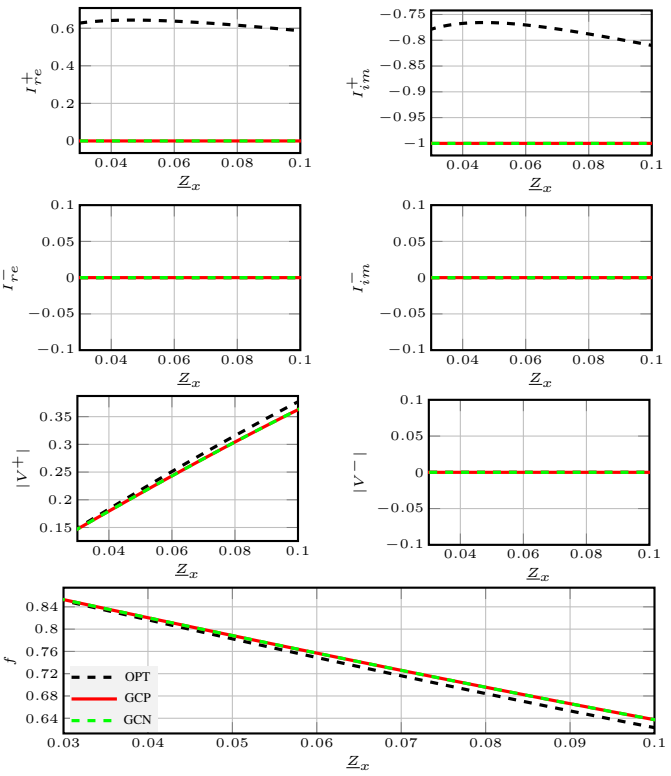

Fig. 5: Influence of the currents for a balanced fault with a varying fault impedance, one-converter case

currents between the real and imaginary parts. The imaginary current remains slightly larger than the real current (in absolute value). This is the main difference between OPT and the grid code implementation found in GCP and GCN. These two strategies always specify a null real current in both sequences, and in this case, they employ their full capability for the imaginary positive sequence current. Therefore, their objective functions and voltage profiles become identical, simply put, because this is a balanced fault.

Significantly different results are obtained in the case of a line to line fault, as shown in Fig. 6. This unbalanced fault causes the optimal currents to be almost null in the positive sequence, so the majority of the current capability is employed for the negative sequence. Severe faults require a large real current (in absolute value), whereas in the case of less extreme faults, the imaginary current tends to the maximum, i.e, 1. Even though the real current is kept at zero for GCP and GCN, their imaginary currents vary significantly across the range of $\underline{Z}_x$ values. GCP tends to approach the results provided by OPT for large $\underline{Z}_x$, whereas GCN evolves on the contrary direction. That is, for low fault impedances, GCP prioritizes injecting current in the positive sequence whereas GCN does the same for the negative sequence, as expected. As a consequence, positive sequence voltages in the case of GCP are initially superior to the ones obtained with GCN, and the contrary applies to the negative sequence voltages. The situation is reversed around $\underline{Z}_x \approx 0.1$. Since the fault is not that severe, much of the current capability is employed in the non-prioritized sequence in order to reach

saturation. In the end, there is an almost constant minimal difference between OPT and GCP, as their objective functions are nearly the same. Therefore, there is not a single optimal solution.

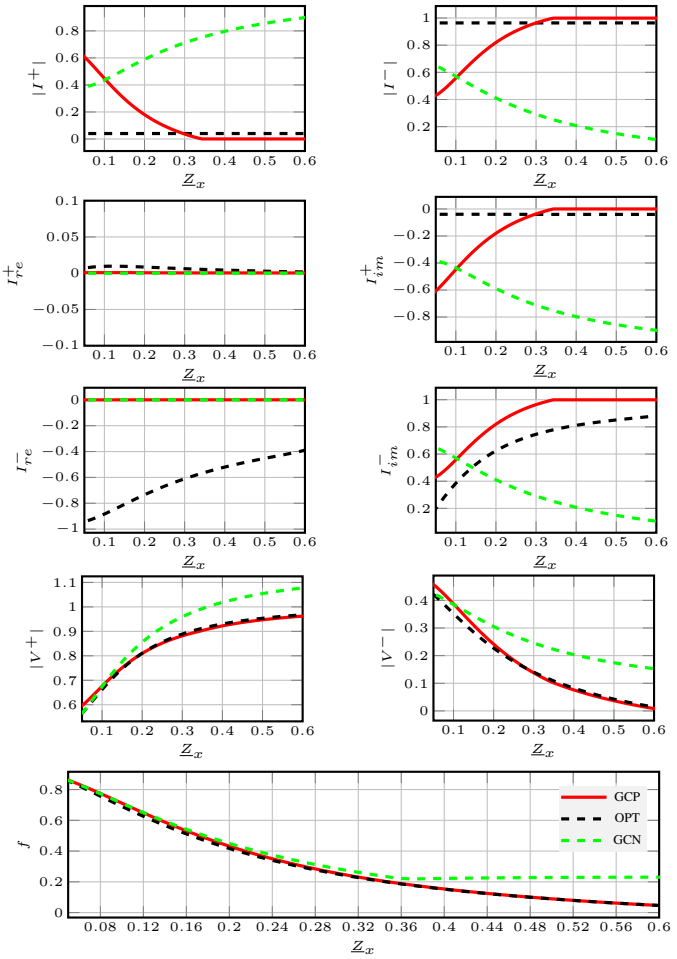

Fig. 6: Influence of the currents for a line to line fault with a varying fault impedance, one-converter case

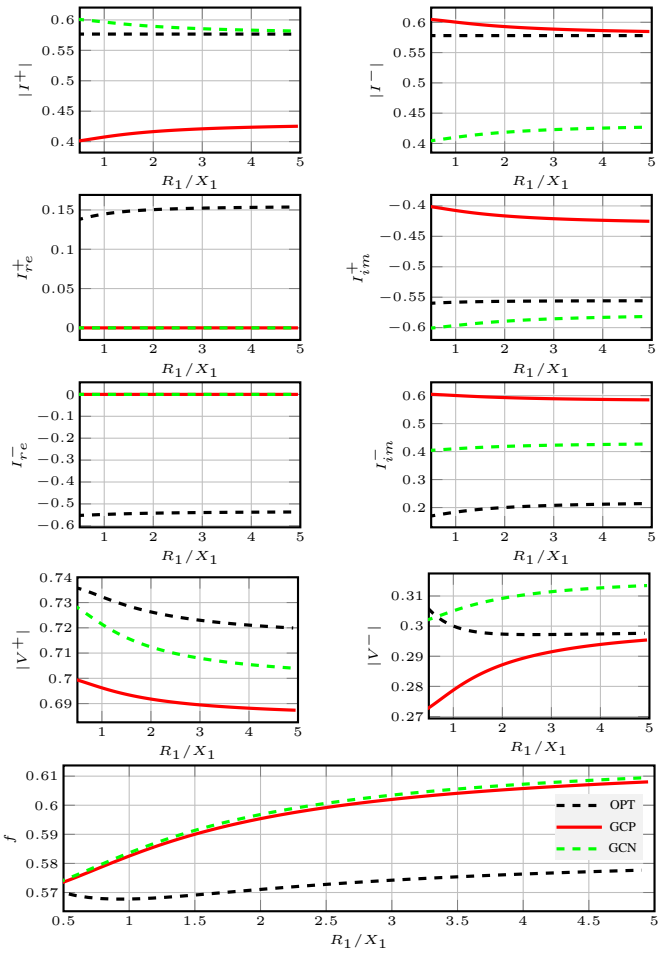

Fig. 7: Influence of the currents for the line to ground fault with a varying R_1/X_1 ratio and a fault impedance $\underline{Z}_{ag} = 0.01$, one-converter case

B. R_1/X_1 variation analysis

The R_1/X_1 variation analysis performs a swept for a range of a varying angle of the $\underline{Z}_{v1}$ impedance, while the absolute value is preserved. The goal of this study is to determine how this affects the distribution of currents between the real and the imaginary part. The results in Fig. 7 for the OPT case show that despite an increase in the resistive part of the impedance, the currents remain nearly constant for all the range of values. Most of the current capability is dedicated to I^+_{im} and I^-_{re}. The converter injects a non-negligible active power, as the injected complex power remains around $0.30 + j0.45$.

For large R_1/X_1 differences between the objective functions of OPT and GCP and GCN are acute due to the incapability of injecting real current. The OPT option achieves a larger positive sequence voltage than both GCP and GCN for all ranges of values. Although the negative sequence voltage obtained with OPT is initially larger, it is further reduced with increases in R_1/X_1, whereas this same voltage tends to grow for GCP and GCN. Despite the fact that GCP prioritizes active current, as the fault is not extreme and it has been imposed that the converter has to operate under saturated conditions, the GCP strategy injects more current in the negative sequence than in the positive sequence. The contrary applies to the GCN option. Therefore, GCN yields larger $|V^+|$ and $|V^-|$ voltages compared to GCP. In the end, the objective function is practically the same for both choices.

C. Cable length variation analysis

Fig. 8 represents the third parametric study regarding single converter systems, which deals with a hypothetical submarine cable modeled with its π equivalent. The data selected to model the cable are extracted from [27] and adapted to per-unit values. Table II presents them. The followed approach to analyze the system is identical to the previous ones, except for the reduction of the set of elements including the cable and the grid. The corresponding Thevenin equivalent is defined by

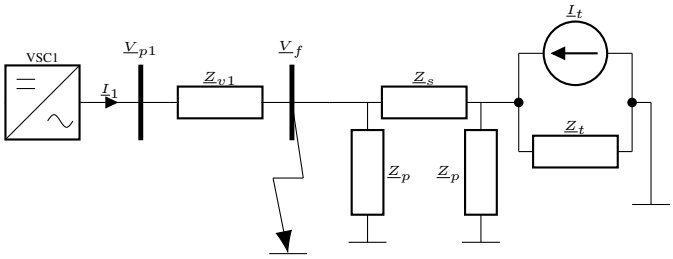

Fig. 8: Single-phase representation of the single converter connected to a system with a cable

TABLE II: System parameters for the one-converter case

Parameter	Value	Units
$\underline{Z}_s$	$6.674 \cdot 10^{-5} + j2.597 \cdot 10^{-4}$	pu/km
$\underline{Z}_p$	$-j77.372$	pu·km

$$\begin{cases} \underline{V}'_t = \frac{\underline{Z}_p \underline{Z}_p}{2\underline{Z}_t\underline{Z}_p + \underline{Z}_p\underline{Z}_s + \underline{Z}_p\underline{Z}_p + \underline{Z}_t\underline{Z}_s} \\ \underline{Z}'_t = \frac{\underline{Z}_p\underline{Z}_p\underline{Z}_t + \underline{Z}_p\underline{Z}_p\underline{Z}_s + \underline{Z}_p\underline{Z}_s\underline{Z}_t}{2\underline{Z}_p\underline{Z}_t + \underline{Z}_s\underline{Z}_p + \underline{Z}_s\underline{Z}_t + \underline{Z}_p\underline{Z}_p} \end{cases} \tag{16}$$

Similarly as before, a Norton equivalent is preferred. The current $\underline{I}'_t$ is simply equal to $\underline{V}'_t/\underline{Z}'_t$, which yields a basic system as the one in Fig. 4.

The analysis performed considers a cable with a varying length, up to 100 km. Its impact on the Thevenin equivalent parameters is shown in Fig. 9. The voltage experiences a subtle increase, while the imaginary part of the equivalent impedance grows considerably with distance, yet the $\Re(\underline{Z}'_t)/\Im(\underline{Z}'_t)$ ratio tends to rise.

The options OPT, GCP and GCN are again evaluated, as depicted in Fig. 10. Increasing the cable distance causes the negative sequence voltage to grow, while the positive sequence voltage also tends to grow. This phenomenon mostly differs from the profiles obtained in Fig. 6 and 7, where both voltages either simultaneously approached the objective value (1 and 0 respectively), or distanced from it. Thus, it makes sense that larger distances imply a lower I^+_{im} current in the case of the grid code implementation, while the less convenient growing negative sequence voltages force an increment in I^-_{im}. Most of the current capability is precisely devoted to this negative sequence imaginary current. The OPT option achieves a more favorable objective function value than GCP and GCN by keeping the positive sequence currents practically constant, increasing I^-_{re} (in absolute value), and decreasing I^-_{im}, which

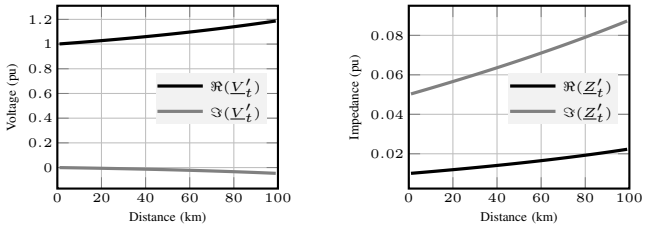

Fig. 9: Thevenin voltage and impedance depending on the cable distance

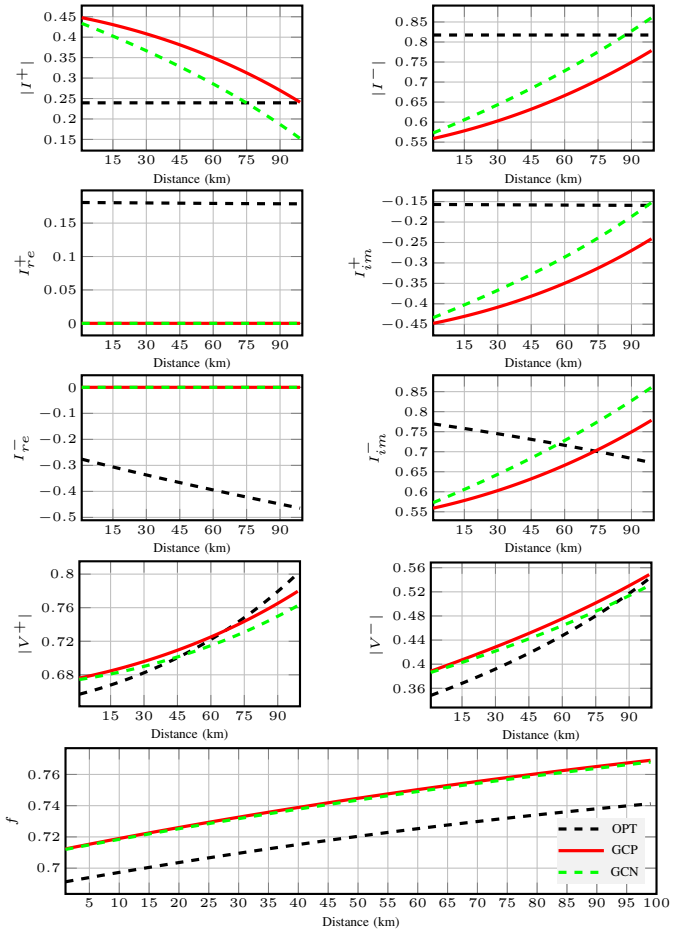

Fig. 10: Influence of the currents for a line to line fault with $\underline{Z}_{ab} = 0.1$ and a varying cable distance, one-converter case

TABLE III: System parameters for the two converter case

Parameter	Value
$\underline{V}_t$	1.00
$I_{\max}$	1.00
$\underline{Z}_{v1}$	$0.01 + j0.05$
$\underline{Z}_{v2}$	$0.02 + j0.06$
$\underline{Z}_t$	$0.01 + j0.1$
$[\lambda^+_1, \lambda^-_1, \lambda^+_2, \lambda^-_2]$	$[1, 1, 1, 1]$

is the inverse trend followed by GCP and GCN. Surprisingly, in the OPT case, the VSC would have to inject a tiny negative active power, that is, this active power should flow from the grid to the converter.

IV. Two-converter case study

A two-converter case is proposed in order to spot the interaction between both converters and compare the performance of the optimization with the grid code rules. Fig. 11 shows a single-phase representation of the system under study. The converters are coupled to the grid by means of slightly different impedances $\underline{Z}_{v1}$ and $\underline{Z}_{v2}$. Table III shows their values together with other input data.

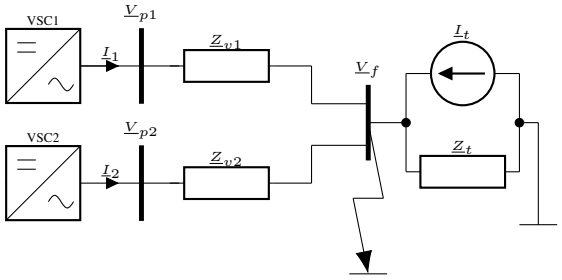

Fig. 11: Single-phase representation of the two-converter system under study

Analogous to the one-converter situation, the optimization problem becomes

$$\begin{aligned} \min_{\underline{I}_1^a,\underline{I}_1^b,\underline{I}_1^c,\underline{I}_2^a,\underline{I}_2^b,\underline{I}_2^c} \quad & \lambda_1^+|(1-|\underline{V}_{p1}^+|)| + \lambda_1^-|(0-|\underline{V}_{p1}^-|)| \\ & + \lambda_2^+|(1-|\underline{V}_{p2}^+|)| + \lambda_2^-|(0-|\underline{V}_{p2}^-|)|, \\ \text{s.t.} \quad & \max(\underline{I}_1^a,\underline{I}_1^b,\underline{I}_1^c) \le I_{\text{max},1} \ , \\ & \max(\underline{I}_2^a,\underline{I}_2^b,\underline{I}_2^c) \le I_{\text{max},2} \end{aligned} \tag{17}$$

where the dependence of the currents on the voltages has been omitted. The application of the grid code is the same as before, in the sense that the injection of current $\underline{I}_1$ only depends on $\underline{V}_{p1}$, and $\underline{I}_2$ is only a function of $\underline{V}_{p2}$.

A. Fault impedance variation analysis

The results associated with a line to ground fault with a varying fault impedance are shown in Fig. 12. Differences in the objective function are negligible for small values of $\underline{Z}_x$, that is, for strong faults. Nevertheless, the converter operates in saturated conditions in all cases. Due to the fact that $\underline{Z}_{v1} \neq \underline{Z}_{v2}$, the distribution of the current capability varies. For instance, in the positive sequence, VSC2 injects more imaginary current (in absolute value), which makes sense considering that $\Im(\underline{Z}_{v2}) > \Im(\underline{Z}_{v1})$. However, the absolute value of I_{im}^- becomes larger for VSC1, which seems counterintuitive. Since the fault is for the most part not extreme ($|V^+| \approx 0.75$ and $|V^-| \approx 0.25$), GCP ends up injecting more negative sequence current whereas GCN injects more positive sequence current. This is translated into having larger positive sequence voltages for GCN and smaller negative sequence voltages for GCP. A similar pattern was observed in Fig. 7. OPT balances both sequences and manages to minimize the objective function.

B. R/X variation analysis

The angle variation of the impedance of connection is applied to only $\underline{Z}_{v1}$ in order to spot more clearly the differences in the distribution of currents between the sequences. For a line to line fault with $\underline{Z}_x = 0.1$, Fig. 13 indicates that since R_2/X_2 is constant, the currents injected by VSC2 experience tiny changes. On the contrary, the currents injected by VSC1 change more significantly. The optimal strategy is to inject null currents in the positive sequence so that all current capability is employed to reduce the negative sequence

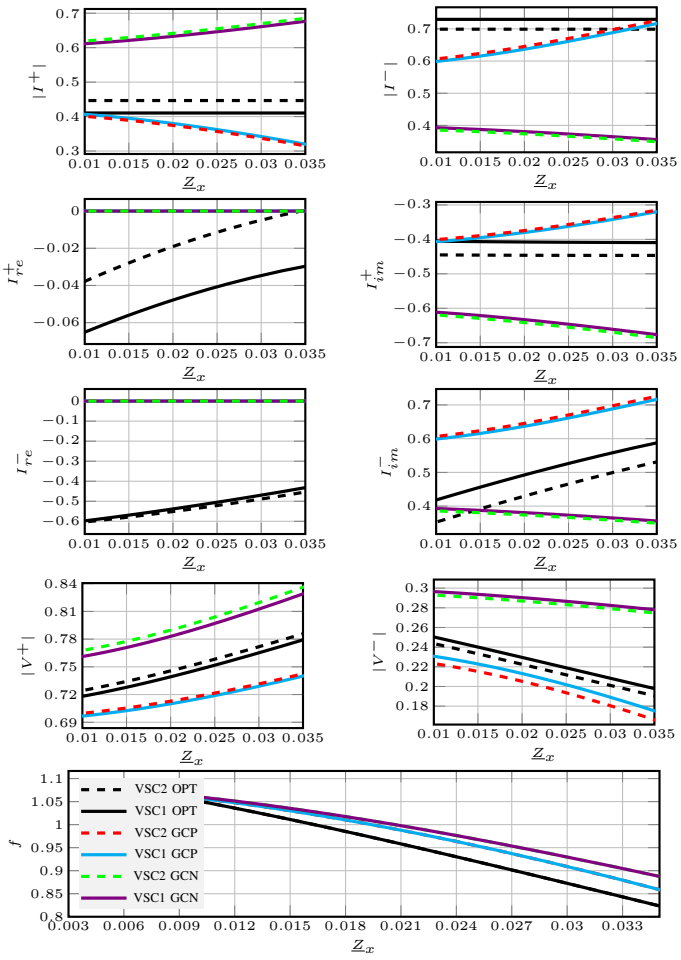

Fig. 12: Influence of the currents for the line to ground fault with a varying fault impedance in a two-converter case

voltage. A similar approach was found to be optimal in the one-converter case, as shown in Fig. 6. As a consequence, the positive sequence voltage in the OPT case becomes smaller than the one obtained for GCP and GCN, yet the reduction on the negative sequence voltage is more substantial, which causes the objective function to be reduced by more than 10%. Out of the multiple faults analyzed in this paper, this is the one where differences in the objective function are larger.

V. Conclusion

This paper has proposed an optimization scheme to improve the voltages under faults. Such strategy has been compared with conventional grid codes, where either positive or negative currents are prioritized and the converter is forced to operate under saturation conditions by only injecting reactive power. Several parameters have been swept, such as the fault impedance, the angle of the interconnecting impedance, and the length of a submarine cable, either for one or two-converter cases. In most situations, the distribution of currents derived from the optimization differs considerably from the currents injected following the grid codes. Yet, the optimization function, which in turn depends on the positive and negative sequence voltages, rarely improves by more than

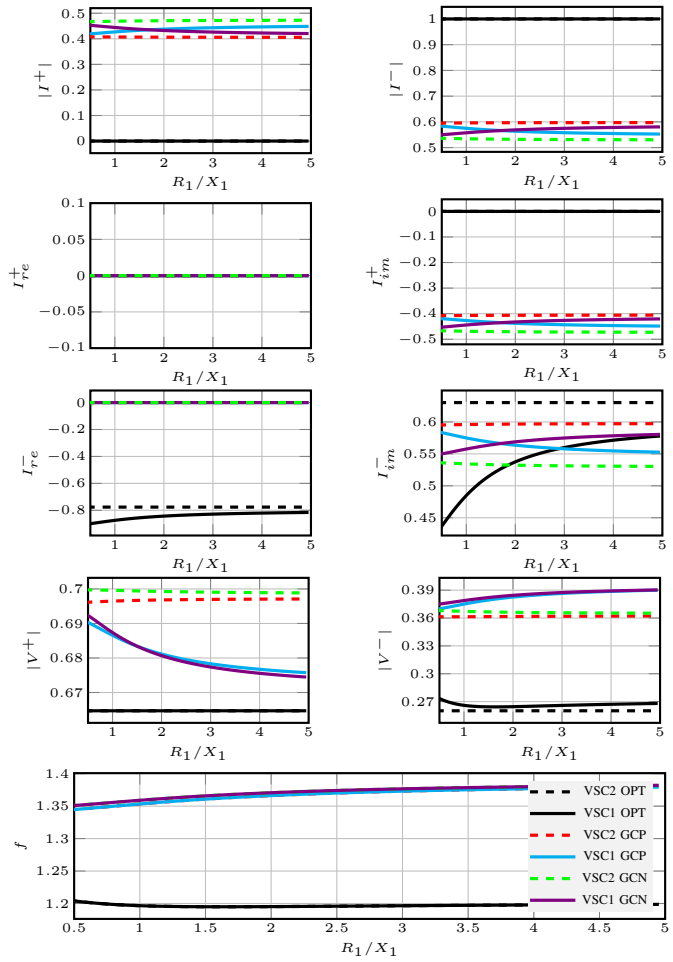

Fig. 13: Influence of the currents for the line to line fault with a varying R_1/X_1 ratio and $\underline{Z}_x = 10$ in a two-converter case

10%. Differences are especially tiny for severe faults. Thus, this work concludes that there are no large improvements to be gained by employing other rules. Grid codes are already near-optimal choices, even if no active power is injected.

Acknowledgment

Fill this.

Appendix

TABLE IV: Grid code constants

Parameter	Value
V^+_{high}	0.9
V^+_{low}	0.4
V^-_{high}	0.6
V^-_{low}	0.1
k_p	2.0
k_n	2.0

References

[1] M. Imhof and G. Andersson, "Power system stability control using voltage source converter based hvdc in power systems with a high penetration of renewables," in *2014 Power Systems Computation Conference*. IEEE, 2014, pp. 1–7.

[2] S. Eren, A. Bakhshai, and P. Jain, "Control of three-phase voltage source inverter for renewable energy applications," in *2011 IEEE 33rd International Telecommunications Energy Conference (INTELEC)*. IEEE, 2011, pp. 1–4.

[3] F. Blaabjerg, Y. Yang, K. Ma, and X. Wang, "Power electronics-the key technology for renewable energy system integration," in *2015 International Conference on Renewable Energy Research and Applications (ICRERA)*. IEEE, 2015, pp. 1618–1626.

[4] A. Abdou, A. Abu-Siada, and H. Pota, "Improving the low voltage ride through of doubly fed induction generator during intermittent voltage source converter faults," *Journal of Renewable and Sustainable Energy*, vol. 5, no. 4, p. 043110, 2013.

[5] J. Morren, *Grid support by power electronic converters of Distributed Generation units*, 2006.

[6] I. Erlich, W. Winter, and A. Dittrich, "Advanced grid requirements for the integration of wind turbines into the german transmission system," in *2006 IEEE Power Engineering Society General Meeting*. IEEE, 2006, pp. 7–pp.

[7] X. Zhang, Z. Wu, M. Hu, X. Li, and G. Lv, "Coordinated control strategies of vsc-hvdc-based wind power systems for low voltage ride through," *energies*, vol. 8, no. 7, pp. 7224–7242, 2015.

[8] M. Mohseni and S. M. Islam, "Review of international grid codes for wind power integration: Diversity, technology and a case for global standard," *Renewable and Sustainable Energy Reviews*, vol. 16, no. 6, pp. 3876–3890, 2012.

[9] M. Tsili and S. Papathanassiou, "A review of grid code technical requirements for wind farms," *IET Renewable power generation*, vol. 3, no. 3, pp. 308–332, 2009.

[10] J. Conroy and R. Watson, "Low-voltage ride-through of a full converter wind turbine with permanent magnet generator," *IET Renewable power generation*, vol. 1, no. 3, pp. 182–189, 2007.

[11] A. Haddadi, I. Kocar, J. Mahseredjian, U. Karaagac, and E. Farantatos, "Negative sequence quantities-based protection under inverter-based resources challenges and impact of the german grid code," *Electric Power Systems Research*, vol. 188, p. 106573, 2020.

[12] A. Camacho, M. Castilla, J. Miret, L. G. de Vicuña, and R. Guzman, "Positive and negative sequence control strategies to maximize the voltage support in resistive–inductive grids during grid faults," *IEEE Transactions on Power Electronics*, vol. 33, no. 6, pp. 5362–5373, 2017.

[13] Red Eléctrica de España. (2016) Información sobre implementación de códigos de red de conexión. textos de los códigos de red de conexió europeos. reglamento 2016/631. [Online]. Available: https://www.esios.ree.es/es/pagina/codigos-red-conexion

[14] A. G. Paspatis and G. C. Konstantopoulos, "Voltage support under grid faults with inherent current limitation for three-phase droop-controlled inverters," *Energies*, vol. 12, no. 6, p. 997, 2019.

[15] A. Camacho, M. Castilla, J. Miret, J. C. Vasquez, and E. Alarcon-Gallo, "Flexible voltage support control for three-phase distributed generation inverters under grid fault," *IEEE transactions on industrial electronics*, vol. 60, no. 4, pp. 1429–1441, 2012.

[16] X. Guo, X. Zhang, B. Wang, W. Wu, and J. M. Guerrero, "Asymmetrical grid fault ride-through strategy of three-phase grid-connected inverter considering network impedance impact in low-voltage grid," *IEEE Transactions on Power Electronics*, vol. 29, no. 3, pp. 1064–1068, 2013.

[17] M. M. Shabestary and Y. A.-R. I. Mohamed, "An analytical method to obtain maximum allowable grid support by using grid-connected converters," *IEEE Transactions on Sustainable Energy*, vol. 7, no. 4, pp. 1558–1571, 2016.

[18] Z. Dai, H. Lin, H. Yin, and Y. Qiu, "A novel method for voltage support control under unbalanced grid faults and grid harmonic voltage disturbances," *IET power Electronics*, vol. 8, no. 8, pp. 1377–1385, 2015.

[19] M. M. Shabestary and Y. A.-R. I. Mohamed, "Asymmetrical ride-through and grid support in converter-interfaced dg units under unbalanced conditions," *IEEE Transactions on Industrial Electronics*, vol. 66, no. 2, pp. 1130–1141, 2018.

[20] M. M. Shabestary, S. Mortazavian, and Y. I. Mohamed, "Overview of voltage support strategies in grid-connected vscs under unbalanced grid faults considering lvrt and hvrt requirements," in *2018 IEEE International Conference on Smart Energy Grid Engineering (SEGE)*. IEEE, 2018, pp. 145–149.

[21] M. T. Andani, H. Pourgharibshahi, Z. Ramezani, and H. Zargarzadeh, "Controller design for voltage-source converter using lqg/ltr," in *2018 IEEE texas power and energy conference (TPEC)*. IEEE, 2018, pp. 1–6.

[22] M. G. Taul, S. Golestan, X. Wang, P. Davari, and F. Blaabjerg, "Modeling of converter synchronization stability under grid faults: The

general case," *IEEE Journal of Emerging and Selected Topics in Power Electronics*, 2020.

[23] C. L. Fortescue, "Method of symmetrical co-ordinates applied to the solution of polyphase networks," *Transactions of the American Institute of Electrical Engineers*, vol. 37, no. 2, pp. 1027–1140, 1918.

[24] M. M. McKerns, L. Strand, T. Sullivan, A. Fang, and M. A. Aivazis, "Building a framework for predictive science," *arXiv preprint arXiv:1202.1056*, 2012.

[25] M. McKerns, P. Hung, and M. Aivazis, "mystic: highly-constrained non-convex optimization and uq, 2009."

[26] National Grid, "The grid code, issue 6, revision 1," https://www.nationalgrideso.com/document/162271/download, 2021.

[27] M. Cheah, "Offshore wind integration through high voltage direct current systems," Ph.D. dissertation, Cardiff University, 2017.